# The Tornadic Vortex Signature: An Update

RODGER A. BROWN AND VINCENT T. WOOD

*NOAA/National Severe Storms Laboratory, Norman, Oklahoma*

(Manuscript received 28 September 2011, in final form 14 December 2011)

ABSTRACT

A tornadic vortex signature (TVS) is a degraded Doppler velocity signature of a tornado that occurs when the core region of a tornado is smaller than the half-power beamwidth of the sampling Doppler radar. Soon after the TVS was discovered in the mid-1970s, simulations were conducted to verify that the signature did indeed represent a tornado. The simulations, which used a uniform reflectivity distribution across a Rankine vortex model, indicated that the extreme positive and negative Doppler velocity values of the signature should be separated by about one half-power beamwidth regardless of tornado size or strength. For a Weather Surveillance Radar-1988 Doppler (WSR-88D) with an effective half-power beamwidth of approximately 1.4° and data collected at 1.0° azimuthal intervals, the two extreme Doppler velocity values should be separated by 1.0°. However, with the recent advent of 0.5° azimuthal sampling (''superresolution'') by WSR-88Ds at lower elevation angles, some of the extreme Doppler velocity values unexpectedly were found to be separated by 0.5° instead of 1.0° azimuthal intervals. To understand this dilemma, the choice of vortex model and reflectivity profile is investigated. It is found that the choice of vortex model does not have a significant effect on the simulation results. However, using a reflectivity profile with a minimum at the vortex center does make a difference. The revised simulations indicate that it is possible for the distance between the peak Doppler velocity values of a TVS to be separated by 0.5° with superresolution data collection.

## 1. Introduction

During the late 1960s and early 1970s, pulsed Doppler radars began to be used to systematically study severe and tornadic thunderstorms in Massachusetts (e.g., Donaldson et al. 1966; Kraus, 1970; Donaldson 1970) and Oklahoma (e.g., Brown et al. 1971, 1973; Burgess and Brown 1973). A breakthrough in Doppler radar identification of tornadoes occurred in 1973 when the National Severe Storm Laboratory's 10-cm wavelength Doppler radar (half-power beamwidth of 0.8°; following convention, the word beamwidth will be used to mean half-power beamwidth throughout the remainder of this paper) in Norman, Oklahoma, detected the presence of a Doppler velocity signature associated with the tornado that struck Union City, Oklahoma, on 24 May 1973 (Burgess et al. 1975; Brown et al. 1978). The signature consisted of extreme positive and negative Doppler velocity values located at adjacent azimuths (separated by 1.0°). The signature was first detected at midlevels in the storm and then strengthened in magnitude as it extended upward and downward. A detailed damage survey indicated that signatures at the lowest elevation angle coincided with the tornado track.

To understand the relationship between a tornado and the Doppler velocity signature, Brown et al. (1978) used the Doppler radar simulator of Zrnić and Doviak (1975) to create Doppler velocity fields for idealized vortices. A Rankine vortex profile (e.g., Rankine 1882) was used to simulate the distribution of tangential velocities within the vortex. The radar reflectivity distribution across the vortex was assumed to be uniform; there were some indications that a weak reflectivity region is associated with the center of a tornado (e.g., Fujita 1981), but it was not apparent at that time how often it occurs or how the reflectivity is distributed relative to the core radius.

The resulting simulated Doppler velocity data indicate that—for tornado core regions smaller than the radar beamwidth—Doppler velocity peaks of opposite sign are expected to occur at azimuthal locations separated by about one beamwidth regardless of tornado size, strength, or distance from the radar (Fig. 1). Since it was not clear from the limited number of available observations whether

*Corresponding author address:* Dr. Rodger A. Brown, National Severe Storms Laboratory, 120 David L. Boren Blvd., Norman, OK 73072.
E-mail: rodger.brown@noaa.gov

DOI: 10.1175/WAF-D-11-00111.1

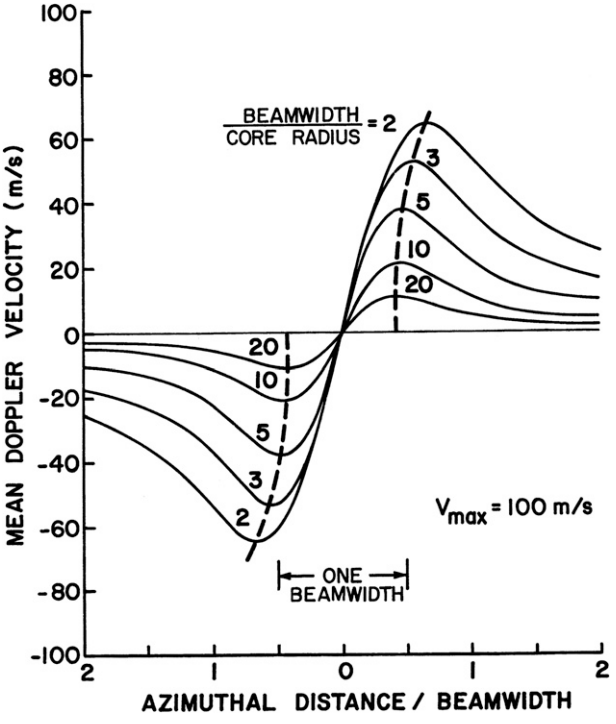


FIG. 1. Simulated azimuthal Doppler velocity profiles through the center of a tornadic vortex signature for various beamwidth to core radius ratios (representing various ranges from the radar for a given vortex). The abscissa is normalized by dividing the azimuthal distance from the vortex center by the radar's beamwidth. The maximum tangential velocity of the Rankine vortex is 100 m $s^{-1}$. The simulations assumed uniform reflectivity across the vortex. [From Brown et al. (1978).]

all tornado-like signatures aloft evolve into tornadoes touching the ground, the signature was called a tornadic vortex signature (TVS).

With the installation of the national network of Weather Surveillance Radar-1988 Dopplers (WSR-88Ds) during the early and mid-1990s, the TVS began to be used operationally by the National Weather Service to identify the presence of tornadoes (e.g., Warning Decision Training Branch 2011). The WSR-88Ds have a nominal antenna beamwidth of about 0.9°. Since the simulations indicated that the peak TVS values should be about one beamwidth apart, the TVS peaks would be separated by 1.0° (adjacent azimuthal sampling intervals) and occasionally by 2.0° [every other azimuthal sampling interval when the center of one azimuthal sampling interval is close to the center of the tornado; e.g., Wood and Brown (1997)]. One should note that the azimuthal sampling interval is independent of the antenna's beamwidth.

In 2008, the azimuthal sampling interval at the lower WSR-88D elevation angles was decreased from 1.0° (legacy resolution) to 0.5° (superresolution) based on simulations and field tests (e.g., Wood et al. 2001; Brown et al. 2002, 2005). Superresolution data collection is accomplished by overlapping 1.0°-wide azimuthal sampling intervals centered at 0.5° azimuthal intervals. With 0.5° azimuthal data collection, one would expect the TVS peaks to be separated by about one beamwidth or 1.0° (every other azimuthal location). However, the peaks occasionally are observed to be separated by only 0.5°—contrary to the simulation results. To help solve this quandary, we repeated the simulations using other vortex models and other reflectivity profiles across the vortices. The findings of these new simulations are discussed in the following sections.

## 2. Doppler radar simulator

For the Doppler radar computations, we used a radar simulator that approximates the characteristics of the WSR-88D (e.g., Wood and Brown 1997). Since a radar antenna moves during the collection of data samples, the meteorological parameters calculated from the samples are somewhat smoothed as if the radar beam were broader than that associated with a stationary antenna; the width of the hypothetical broadened beam is called the effective beamwidth (e.g., Doviak and Zrnić 1993, 193–197). The effective beamwidth (EBW) for a given radar can be determined from the beamwidth of the antenna and the azimuthal sampling interval (e.g., Fig. 1 of Brown et al. 2002); nominal values for the WSR-88D are listed in Table 1 along with some of the simulation results. A pulse depth of 0.25 km and an effective beamwidth of 1.0° were used for the simulations; since the results are normalized relative to effective beamwidth, the value chosen for the effective beamwidth is not crucial.

For simplicity, the radar scanned horizontally through the vortex only at the range of the vortex center from the radar. Furthermore, we assumed that the tangential velocity and reflectivity profiles across the vortex were constant with height, so that, instead of making measurements throughout the two-dimensional (azimuth–elevation) beam, we made measurements only in the one-dimensional azimuthal direction through the center of the beam. Since the main lobe of radiation produced by the WSR-88D antenna is approximately Gaussian shaped and its width is 2.5–3 times the width at the half-power point (e.g., Doviak and Zrnić 1993, chapter 7), we assumed that the simulated main lobe was Gaussian shaped and equal to 3 times the effective beamwidth; the much weaker side lobes were not simulated.

In reality, radar parameters are computed from 10s of transmitted pulses. Instead, for the simulations, we computed the reflectivity and mean Doppler velocity from data at 101 evenly distributed points across the full one-dimensional main lobe. A continuous distribution

TABLE 1. Nominal WSR-88D characteristics including EBW for legacy and superresolution azimuthal data collection. Also listed are the simulation results for the ratio of TVS diameter to EBW and the azimuthal separation of TVS peak values (TVS ΔAz) based on a Burgers–Rott tangential velocity profile and a weak-reflectivity eye at the center of the vortex (from Fig. 5).

| WSR-88D resolution | Azimuthal increment (°) | Antenna half-power beamwidth (°) | Effective half-power beamwidth (°) | TVS diameter / EBW | TVS ΔAz |
|---|---|---|---|---|---|
| Legacy | 1.0 | 0.9 | 1.4 | 0.65–0.9 | 1.0° (2.0°)* |
| Super | 0.5 | 0.9 | 1.0 | 0.65–0.9 | 0.5°, 1.0° |

* When the center of the radar beam passes through the center of the tornado, the peak legacy Doppler velocity values will be 2.0° apart.

of mean Doppler velocity and reflectivity values was then derived by positioning the antenna at 0.001° increments across the model vortex.

## 3. Results using four vortex models

To illustrate the influence of various vortex models on TVSs, we considered the simulation results of Wood and Brown (2011). They used a uniform reflectivity profile when investigating four vortex models: the Rankine, Burgers–Rott, Sullivan, and modified Sullivan vortex models, as shown in Fig. 2. Details of these vortex models are discussed by Davies-Jones (1986) and Wood and White (2011), for example. The Rankine and Burgers–Rott models represent vortices that are associated with updrafts, while the two Sullivan models with the broader

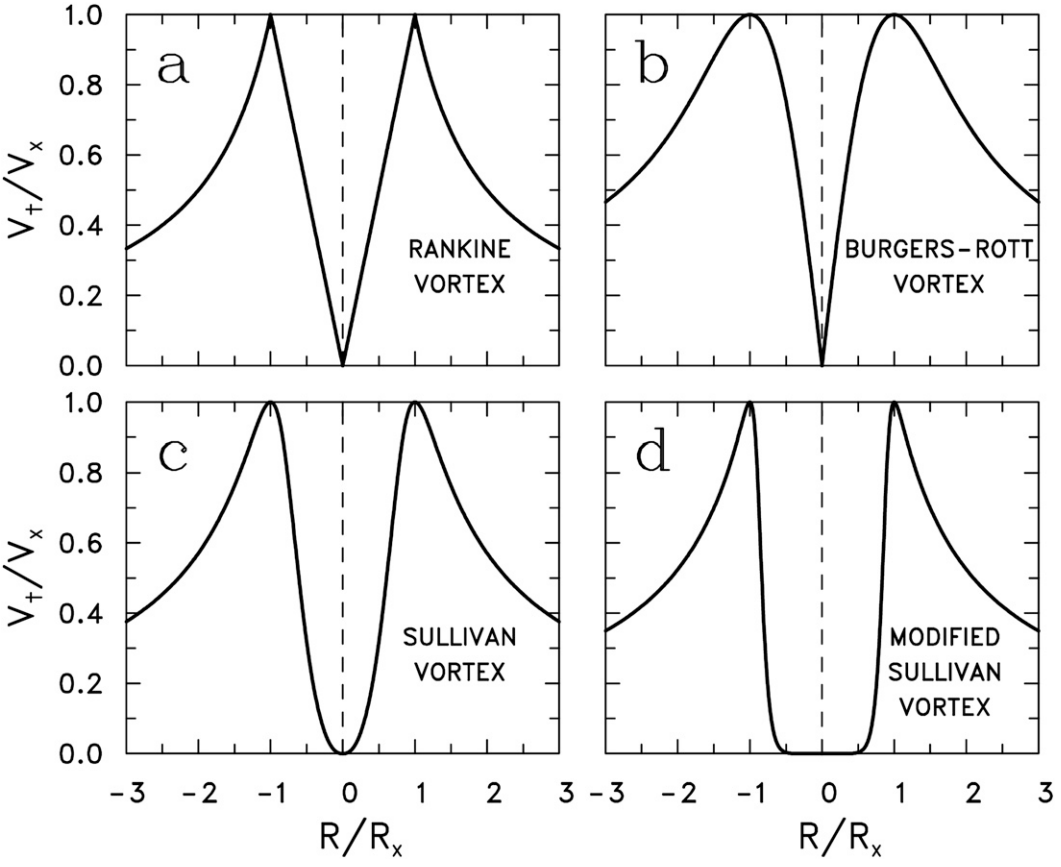


FIG. 2. Tangential velocity profiles for four idealized vortex models. The Rankine and Burgers–Rott vortices are associated with updrafts (one-celled vortices) and the two Sullivan vortices are associated with a central downdraft surrounded by an updraft (two-celled vortices); the modified Sullivan vortex represents an extreme case with an unusually wide downdraft. Tangential velocities ($V_t$) are normalized by the peak tangential velocity ($V_x$) that occurs at the core radius $R_x$. [From Wood and Brown (2011).]

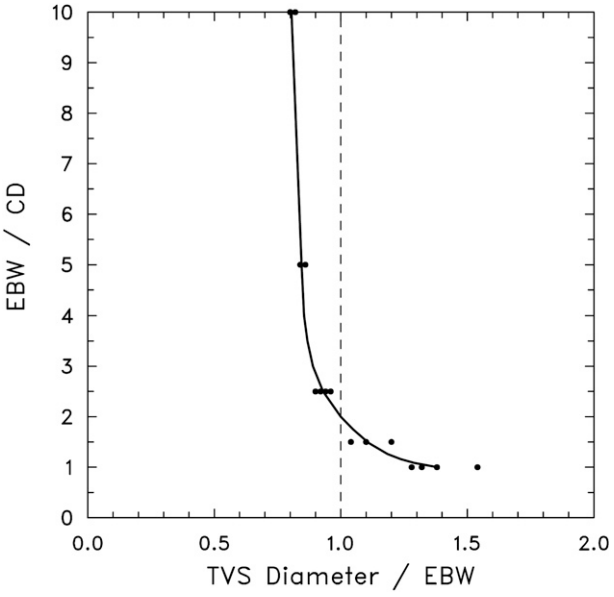


FIG. 3. Distribution of TVS diameter normalized by the EBW as a function of various effective beamwidth to true vortex CD ratios for a reflectivity profile that is uniform across the vortex. The dots from left to right at a given EBW–CD value represent the Rankine, Burgers–Rott, Sullivan, and modified Sullivan vortices, respectively. The curve represents the mean value of TVS diameter/EBW as a function of EBW/CD. [From Wood and Brown (2011).]

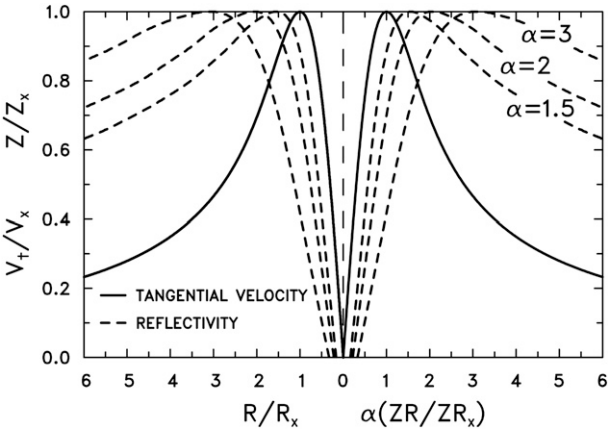


FIG. 4. Relationship of the peaks of three normalized reflectivity profiles (relative to the peak value $Z_x$) and the normalized Burgers–Rott tangential velocity profile (relative to the peak value $V_x$) as a function of radius (ZR, $R$) from the vortex center normalized by the radius of the respective peak values ($ZR_x$, $R_x$); ZR is the radius of the reflectivity profile and $R$ is the radius of the tangential velocity profile. The parameter $\alpha$ is the ratio $ZR_x/R_x$, indicating the radius of peak reflectivity relative to the radius of peak tangential velocity.

regions of zero tangential velocities at the vortex center represent vortices associated with a central downdraft surrounded by an annular updraft. These models do not represent asymmetric vortices or vortices that contain subvortices; however, such details become immaterial when the radar beam is significantly larger than the vortex.

The Wood and Brown (2011) findings are summarized in Fig. 3. The data points represent the ratios of the diameter between the positive and negative peaks of the TVS profile divided by the EBW plotted as a function of effective beamwidth relative to the true vortex core diameter (CD). For effective beamwidths greater than the vortex core diameter (i.e., ratios greater than 1.0), the mean TVS diameter (solid curve) is between 0.8 and 1.3 times the effective beamwidth. Other than the extreme modified Sullivan vortex (the rightmost of the dots in Fig. 3), the normalized TVS diameters are so similar for each EBW–CD ratio that one can reasonably conclude that the choice of vortex model does not significantly affect the distance between the Doppler velocity peaks of a TVS for a given radar's effective beamwidth.

## 4. Results using two types of reflectivity profiles

With the choice of vortex model not affecting the TVS, we compared the TVSs associated with two different types of reflectivity profiles: one with uniform reflectivity and the other with nonuniform reflectivity having a weak-reflectivity eye at the center of the tornado representing the centrifuging of radar-detectable particles. We chose the Burgers–Rott vortex model to represent the tornado's tangential velocity profile because it is a good fit to Doppler velocity measurements made by mobile Doppler radars close to tornadoes (e.g., Bluestein et al. 2007; Tanamachi et al. 2007; Kosiba and Wurman 2010). Since Doppler radar measurements reveal a variety of relationships between the tangential velocity and reflectivity profiles as a function of both height and tornado strength (e.g., Wakimoto and Martner 1992; Wurman and Gill 2000; Bluestein 2005; Bluestein et al. 2007; Wakimoto et al. 2011), three reflectivity profiles were chosen to represent the range of relationships, with the radius of maximum reflectivity ranging from 1.5 to 3.0 times the radius of peak tangential velocity. The relationships between the Burgers–Rott tangential velocity profile and the weak-reflectivity–eye profiles are shown in Fig. 4.

The simulation results in Fig. 5 show that there is a meaningful difference in the normalized TVS diameters between the two types of reflectivity profiles when the effective beamwidth is less than approximately 2.5–4.0 times wider than the tornado's core diameter; the larger the tornado, the greater the distance from the radar where this situation occurs. With the presence of a reflectivity eye, TVS diameters are about 0.65–0.9 times the effective beamwidth, while for uniform reflectivity the

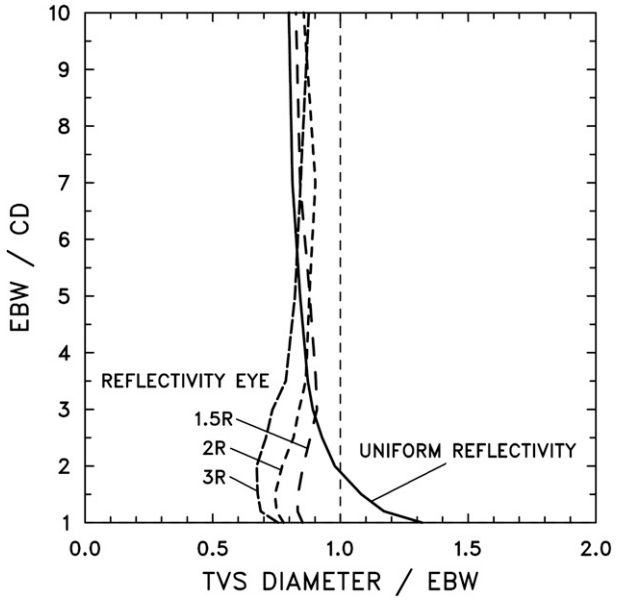


FIG. 5. Simulated TVS diameter relative to the EBW for two types of reflectivity profiles across a Burgers–Rott vortex as a function of the ratio of the effective beamwidth to the true CD of the vortex. The three dashed curves represent reflectivity profiles that have a minimum reflectivity eye at the center of the vortex; 1.5*R*, 2*R*, and 3*R* represent profiles where the radii of the peak reflectivities are 1.5, 2, and 3 times farther from the vortex center than the radius of the peak tangential velocity (see Fig. 4). The Doppler velocity signature is defined as a TVS when the effective beamwidth is greater than the core diameter of the vortex.

diameters are about 0.9–1.3 times the effective beamwidth. For superresolution WSR-88D data collection with an antenna beamwidth of 0.9° and azimuthal sampling interval of 0.5°, the effective beamwidth is 1.0° (e.g., Brown et al. 2002). In this situation, where we expect peak TVS values to be 0.65°–0.9° apart with minimum reflectivity at the center of a tornado, it is entirely reasonable for extreme TVS values to occur occasionally at adjacent azimuths separated by 0.5°. The original 1970s simulations of Brown et al. (1978), with the assumption of uniform reflectivity across the vortex, results in misleading expectations concerning superresolution data collection at shorter distances from a radar.

At greater distances from the radar, where the effective beamwidth is larger than approximately 2.5–4.0 times the tornado core diameter, the choice of reflectivity profile does not significantly affect the size of the TVS, with the distance between the extreme WSR-88D Doppler velocity values being equal to 0.8–0.9 times the effective beamwidth (Fig. 5). For both legacy resolution with 1.0° azimuthal sampling interval (EBW = 1.4°) and superresolution with 0.5° azimuthal sampling interval (EBW = 1.0°), one would expect the peaks to be 1.0° apart (Table 1).

## 5. Concluding discussion

The simulations of Brown et al. (1978) indicate that the peak Doppler velocities (opposite signs) of a tornadic vortex signature should occur at about one beamwidth separation when using the Rankine vortex profile and uniform reflectivity. For legacy WSR-88D data collection at 1.0° azimuthal intervals with an effective beamwidth of 1.4°, one expects the peak velocities to be separated by 1.0° (adjacent azimuths) or occasionally at 2.0° (every other azimuth). This is what is routinely observed. With the recent advent of superresolution data collection (azimuthal increments of 0.5°) at lower elevation angles, the effective beamwidth is 1.0°; so, one would expect the peak Doppler velocity values also to be separated by 1.0°. However, at times, the peaks are observed to be separated by 0.5° instead.

To understand this dilemma, we investigated alternative vortex models and reflectivity profiles. Using four different vortex models having a common reflectivity profile (uniform), the choice of vortex model did not have a major effect on the simulation results. Using two different types of reflectivity profiles (uniform and minimum reflectivity at the vortex center) having a common vortex model (Burgers–Rott), we found that there was a difference when the effective beamwidth was less than approximately 2.5–4.0 times larger than the vortex's core diameter. With the presence of a reflectivity minimum (resulting from centrifuged radar targets), the simulations indicate that it is possible for the distance between superresolution peak Doppler velocity values to be separated by 0.5°. However, when the effective beamwidth is greater than approximately 2.5–4.0 times the core diameter, the peak values are expected to have an azimuthal separation of 1.0° for both legacy resolution (one azimuthal increment) and superresolution (two azimuthal increments) data collection.

*Acknowledgments.* Discussions with James LaDue of the National Weather Service's Warning Decision Training Branch led to the realization that we needed to investigate the influence of various tornado vortex models and reflectivity profiles on the tornadic vortex signature. We appreciate comments on the manuscript by Travis Smith and the anonymous reviewers.

REFERENCES

Bluestein, H. B., 2005: A review of ground-based, mobile, W-band Doppler radar observations of tornadoes and dust devils. *Dyn. Atmos. Oceans,* **40,** 163–188.

——, C. C. Weiss, M. M. French, E. M. Holthaus, and R. L. Tanamachi, 2007: The structure of tornadoes near Attica, Kansas, on 12 May 2004: High-resolution, mobile, Doppler radar observations. *Mon. Wea. Rev.,* **135,** 475–506.

Brown, R. A., W. C. Bumgarner, K. C. Crawford, and D. Sirmans, 1971: Preliminary Doppler velocity measurements in a developing radar hook echo. *Bull. Amer. Meteor. Soc.,* **52,** 1186–1188.

——, D. W. Burgess, and K. C. Crawford, 1973: Twin tornado cyclones within a severe thunderstorms: Single Doppler radar observations. *Weatherwise,* **26,** 63–69, 71.

——, L. R. Lemon, and D. W. Burgess, 1978: Tornado detection by pulsed Doppler radar. *Mon. Wea. Rev.,* **106,** 29–38.

——, V. T. Wood, and D. Sirmans, 2002: Improved tornado detection using simulated and actual WSR-88D data with enhanced resolution. *J. Atmos. Oceanic Technol.,* **19,** 1759–1771.

——, B. A. Flickinger, E. Forren, D. M. Schultz, D. Sirmans, P. L. Spencer, V. T. Wood, and C. L. Ziegler, 2005: Improved detection of severe storms using experimental fine–resolution WSR-88D measurements. *Wea. Forecasting,* **20,** 3–14.

Burgess, D. W., and R. A. Brown, 1973: The structure of a severe right-moving thunderstorm: New single Doppler radar evidence. Preprints, *Eighth Conf. on Severe Local Storms,* Denver, CO, Amer. Meteor. Soc., 40–43.

——, L. R. Lemon, and R. A. Brown, 1975: Tornado characteristics revealed by Doppler radar. *Geophys. Res. Lett.,* **2,** 183–184.

Davies-Jones, R. P., 1986: Tornado dynamics. *Thunderstorm Morphology and Dynamics,* 2nd ed., E. Kessler, Ed., University of Oklahoma Press, 197–236.

Donaldson, R. J., Jr., 1970: Vortex signature recognition by a Doppler radar. *J. Appl. Meteor.,* **9,** 661–670.

——, G. M. Armstrong, and D. Atlas, 1966: Doppler measurements of horizontal and vertical motions in a paired instability line. Preprints, *12th Conf. on Radar Meteorology,* Norman, OK, Amer. Meteor. Soc., 392–397.

Doviak, R. J., and D. S. Zrnić, 1993: *Doppler Radar and Weather Observations*. 2nd ed. Academic Press, 562 pp.

Fujita, T. T., 1981: Tornadoes and downbursts in the context of generalized planetary scales. *J. Atmos. Sci.,* **38,** 1511–1534.

Kosiba, K., and J. Wurman, 2010: The three-dimensional axisymmetric wind field structure of the Spencer, South Dakota, 1998 tornado. *J. Atmos. Sci.,* **67,** 3074–3083.

Kraus, M. J., 1970: Doppler radar investigation of flow patterns within severe thunderstorms. Preprints, *14th Radar Meteor. Conf.,* Tucson, AZ, Amer. Meteor. Soc., 127–132.

Rankine, W. J. M., 1882: *A Manual of Applied Physics*. 10th ed. Charles Griffin and Co., 663 pp.

Tanamachi, R. L., H. B. Bluestein, W.-C. Lee, M. Bell, and A. Pazmany, 2007: Ground-based velocity track display (GBVTD) analysis of W-band Doppler radar data in a tornado near Stockton, Kansas, on 15 May 1999. *Mon. Wea. Rev.,* **135,** 783–800.

Wakimoto, R. M., and B. E. Martner, 1992: Observations of a Colorado tornado. Part II: Combined photogrammetric and Doppler radar analysis. *Mon. Wea. Rev.,* **120,** 522–543.

——, N. T. Atkins, and J. Wurman, 2011: The LaGrange tornado during VORTEX2. Part I: Photogrammetric analysis of the tornado combined with single-Doppler radar data. *Mon. Wea. Rev.,* **139,** 2233–2258.

Warning Decision Training Branch, cited 2011: Distance learning operations course. Topic 5: Base and derived products. [Available online at http://www.wdtb.noaa.gov/courses/dloc/documentation/DLOC_FY11_Topic5.pdf.]

Wood, V. T., and R. A. Brown, 1997: Effects of radar sampling on single-Doppler velocity signatures of mesocyclones and tornadoes. *Wea. Forecasting,* **12,** 928–938.

——, and ——, 2011: Simulated tornadic vortex signatures of tornado-like vortices having one- and two-celled structures. *J. Appl. Meteor. Climatol.,* **50,** 2338–2342.

——, and L. W. White, 2011: A new parametric model of vortex tangential-wind profiles: Development, testing, and verification. *J. Atmos. Sci.,* **68,** 990–1006.

——, R. A. Brown, and D. Sirmans, 2001: Technique for improving detection of WSR-88D mesocyclone signatures by increasing angular sampling. *Wea. Forecasting,* **16,** 177–184.

Wurman, J., and S. Gill, 2000: Finescale radar observations of the Dimmitt, Texas (2 June 1995), tornado. *Mon. Wea. Rev.,* **128,** 2135–2164.

Zrnić, D. S., and R. J. Doviak, 1975: Velocity spectra of vortices scanned by a pulse-Doppler radar. *J. Appl. Meteor.,* **14,** 1531–1539.